AFRL-AFOSR-JP-TR-2024-0027

Stable Li metal anode for high-capacity rechargeable batteries

Suk Jun Kim
KOREATECH Industry-University Cooperation Foundation
1600 Chungjeol-ro, Byeongcheon-myeon DongNam-gu
Cheonan, Chungnam, , 31253
KR

12/12/2023
Final Technical Report

Air Force Research Laboratory
Air Force Office of Scientific Research
Asian Office of Aerospace Research and Development
Unit 45002, APO AP 96338-5002

REPORT DOCUMENTATION PAGE

PLEASE DO NOT RETURN YOUR FORM TO THE ABOVE ORGANIZATION.

1. REPORT DATE	2. REPORT TYPE	3. DATES COVERED	
20231212	Final	START DATE 20200904	END DATE 20220903

4. TITLE AND SUBTITLE
Stable Li metal anode for high-capacity rechargeable batteries

5a. CONTRACT NUMBER	5b. GRANT NUMBER	5c. PROGRAM ELEMENT NUMBER
	FA2386-20-1-4081	61102F
5d. PROJECT NUMBER	**5e. TASK NUMBER**	**5f. WORK UNIT NUMBER**

6. AUTHOR(S)
Suk Jun Kim

7. PERFORMING ORGANIZATION NAME(S) AND ADDRESS(ES)
KOREATECH Industry-University Cooperation Foundation
1600 Chungjeol-ro, Byeongcheon-myeon DongNam-gu
Cheonan, Chungnam 31253
KR

8. PERFORMING ORGANIZATION REPORT NUMBER

9. SPONSORING/MONITORING AGENCY NAME(S) AND ADDRESS(ES)	10. SPONSOR/MONITOR'S ACRONYM(S)	11. SPONSOR/MONITOR'S REPORT NUMBER(S)
AOARD UNIT 45002 APO AP 96338-5002	AFRL/AFOSR IOA	AFRL-AFOSR-JP-TR-2024-0027

12. DISTRIBUTION/AVAILABILITY STATEMENT
A Distribution Unlimited: PB Public Release

13. SUPPLEMENTARY NOTES

14. ABSTRACT
The purpose of this project is to develop a novel Li metal anode that has a high energy density and long lifetime for use in rechargeable batteries. Li is a very promising anode material because of its extremely high theoretical specific capacity (3,860 mAh/g) and low redox potential (-3.04 vs standard hydrogen electrode). However, it has not been commercialized in the last forty years because of the uncontrolled growth of Li dendrites, which grow from the Li anode toward the cathode during cycling. When the anode comes into contact with the cathode via the dendrites, it short-circuits and this results in the failure of the rechargeable batteries. Two strategies that will be employed in this project to solve the problem of dendrite growth are (1) the development of coating materials for the Li metal and (2) the fabrication of Li metal-framework composites. Optimal coating materials will be investigated from among the 2-dimensional (2D) transition metal dichalcogenide materials. Li metal composites will be fabricated using porous materials such as graphite powders and carbon fibers. Finally, the Li metal composites will be coated with the 2D materials. In addition, we also tested optical properties of the 2D
materials, which was developed for Li ion batteries, to evaluate the possibility of utilization of the 2D materials as transparent electrodes.

15. SUBJECT TERMS

16. SECURITY CLASSIFICATION OF:			17. LIMITATION OF ABSTRACT	18. NUMBER OF PAGES
a. REPORT U	b. ABSTRACT U	c. THIS PAGE U	SAR	16

19a. NAME OF RESPONSIBLE PERSON	19b. PHONE NUMBER *(Include area code)*
TONY KIM	315-227-7008

Standard Form 298 (Rev.5/2020)
Prescribed by ANSI Std. Z39.18

Final Performance Report (2020-2022)

Project title: Stable Li metal anode for high-capacity rechargeable batteries

AWARD No. FA2386-20-1-4081

Principal investigator:

Prof. Suk Jun Kim

Korea University of Technology and Education

Email: skim@koreatech.ac.kr, Phone: +82-41-560-1328, Fax: +82-41-560-1303

Address: 1600 CHUNGJEOL-RO, BYEONGCHEON-MYEON DONGNAMGU CHEONAN 31253 KOREA, REPUBLIC OF

---

1. Accomplishments

Published papers

J.H. Lee, H.J. Park, C.E. Im, J.G. Kim, D.E. Gu, S.J. Kim*, "Effect of Co-Solvent Percentages on the Exfoliation Rate of NiTe2 Thin Film for Transparent Electrodes", Korean J. Met. Mater 59, 1, 2021

J. H. Lee, Y. G. Cho, D. E. Gu, S. J. Kim*, "2D $PdTe_2$ Thin-Film-Coated Current Collectors for Long-Cycling Anode-Free Rechargeable Batteries", ACS Appl. Mater. Interfaces 14, 15080, 2022

C. Y. Im, J. G. Kim, M. Y. Kwon, S. J. Kim*, "The Effect of Solvent Mixing Ratios on the Exfoliation of 2D $NiTe_2$ Thin Films for Transparent Electrodes" Electron. Mater. Lett. 18, 361, 2022

Submitted patent

J. H. Lee, S. J. Kim "Anode-free rechargeable lithium metal battery comprising an ion conductive layer and transition metal dichalcogenide layer and manufacturing method thereof" submission date: 07/22/2021 (KR1020210096212)

(US17/524,308)

(CN 202111334446.4)

J. G. Kim, D. E. Gu, S. J. Kim" Anode-free Lithium Secondary Battery, Lithium Metal Secondary Battery, Lithium Metal Battery And Solid-state Secondary Battery Have Amorphous Metal Alloy Coating Layer" submission date: 11/07/2022

(KR1020220147409)

In preparation paper

J. G. Kim, D. E. Gu, S.J. Kim* “Exploiting Zr-based metallic glass thin film for anode-free lithium metal batteries”

2. Technical Progress

(1) Anode-free lithium metal batteries

Introduction

Anode-free rechargeable lithium metal batteries (AFLBs) have been proposed and intensively studied to achieve high energy density that is essential to maximize the driving range of electric vehicles. In an AFLB, Li ions deintercalated from cathode are electroplated onto anode current collector (CC) because no host materials such as graphite exist. Once it is firstly charged, the AFLB works as a Li metal battery yet it has no excess lithium. At successive discharging process, Li on the CC is stripped back to the cathode. Removal of the host materials on the anode side increases its energy density and simplifies the manufacturing process, yet lower Coulombic efficiency (CE) and formation of Li dendrite decrease long-term cycle stability. The dendrite growth and bad morphology of the plated Li on CC is attributed to high lithium nucleation overpotential on CC. Nucleation overpotential is an energy barrier that should be overcome when Li metal is plated on CC. Higher nucleation overpotential generally result in more uneven morphology of the Li deposits, and the uneven deposition promotes dendrite growth because of non-uniform current flux. The dendritic growth of Li leads to enlarge the plated lithium’s surface area per volume where passivating solid-electrolyte interphase (SEI) forms. If the SEI is unstable, it is easy to crack during cycling and leads to forming new SEI layers. The continual formation of SEI results in consumption of Li and electrolyte and an accumulation of dead Li that eventually decreases CE. To overcome these weaknesses, many researchers have attempted to engineer two different interfaces individually: between electrolyte and CC or electrolyte and plated Li. These interfaces influence the nucleation and growth of Li on CC thermodynamically and kinetically. The methods for engineering the interfaces can be largely categorized into three ways: coating CC, modifying 3D structure of CC, and tailoring composition of electrolyte. First, coating CC with organic and inorganic materials and 2D materials such as multilayer graphene and h-BN are studied. The coatings provide uniform current density over the electrode and reduce the nucleation overpotential. A uniform current density distribution minimizes dendritic growth and reduced nucleation overpotential increases size of Li nuclei on CC that leads to smooth top surface of the Li deposits. Second, 3D structure of CC was modified in order to extend electroactive surface area that reduces local current density over the entire CC. The first and second strategies are categorized into modification of the interface between electrolyte and CC. Third, electrolyte was tuned by adding Li salts or/and additives, inventing new solvents, and using solid state electrolyte instead of liquid electrolyte. The tuned electrolytes induce formation of stable SEI, so that the third strategy is to modify the interface between electrolyte and plated Li.

In this study, we successfully demonstrate $PdTe_2$ thin film as an outstanding artificial SEI for CC in anode-free lithium-ion batteries. The $PdTe_2$ coating substantially reduced overpotential for Li nucleation that led

to uniformly distributed nucleation sites for Li plating. Furthermore, in-situ heating during $PdTe_2$ deposition led to the improvement of capacity retention by the formation of CuTe phase at the interface between $PdTe_2$ and the CC. The CuTe phase worked as a glue between $PdTe_2$ and CC (See Scheme 1). $PdTe_2$ is one of transition metal dichalcogenides (TMDs) which are MX_2 (M = transition metal, X = S, Se, Te). TMDs are also 2-dimensional (2D) material and have been investigated as anode material itself in lithium ion batteries. However, the TMD anodes have spontaneous aggregation and unstable electrochemistry during the conversion reaction so the performance is extremely limited. So other methods like fabricating the composite with carbon based materials and MoS_2 coated lithium metal anode were reported. Particularly, Cha et al. reported that the outstanding performance of MoS_2 coated lithium metal anode was attributed to the phase transformation from semiconductor to metal during cycles. Li ions reach MoS_2 and diffused from electrolyte through MoS_2 and plate between MoS_2 thin film and Li metal anode. In contrast, Li ions just plate on the $PdTe_2$ surface during charging due to its metallic property.

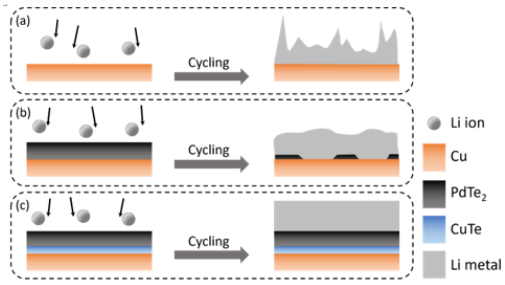

Scheme 1. Difference in morphology of plated lithium on the Cu current collector (a) without $PdTe_2$, (b) with $PdTe_2$, and (c) with $PdTe_2$ and CuTe layers.

Coating of $PdTe_2$ on copper current collectors

5 to 15 nm-thick $PdTe_2$ thin films were uniformly deposited on the CC by magnetron sputtering technique as shown in Figure 1. $PdTe_2$ thin film can be observed with bare eyes and smooth surface was confirmed with SEM. Roughness caused by rolling process on the bare Cu is visible and it still remains after $PdTe_2$ deposition. EDX confirms that Pd and Te elements are uniformly distributed.

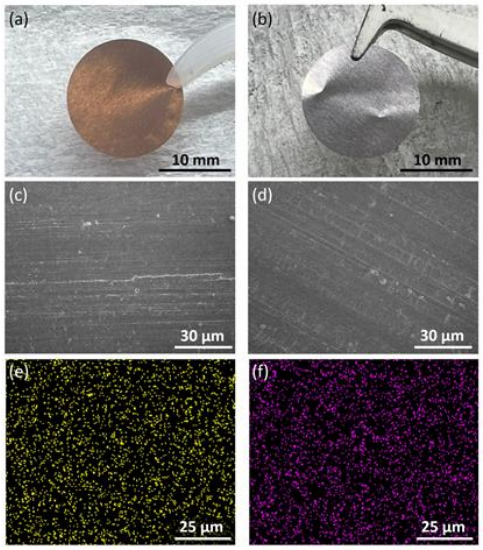

Figure 1. Digital images of (a) bare Cu, (b) $PdTe_2$ coated Cu, SEM images of (c) bare Cu, (d) $PdTe_2$ coated Cu, EDS mapping of (e) Pd and (f) Te

Coulombic efficiency of $PdTe_2$ coated CC

The thickness of $PdTe_2$ layer and heating the CC influence on Coulombic efficiency (CE). The $PdTe_2$ layers with the thickness of 6 nm, 9 nm, and 15 nm were deposited on Cu CC by magnetron sputtering. During the sputtering process, the CC was heated in-situ at 200 C and their CCs were compared to the ones coated without heating. CE was analyzed using Li metal as the counter electrode. The coating tended to improve CE and the CC with thinner coating showed better CE stability as shown in Figure 2a. The CE with 6 nm $PdTe_2$ (6-CC) was stable up to about 80 cycles while the CE of CC with 9 nm (9-CC) and 15 nm PdTe2 (15-CC) dropped after 60 cycles and 45 cycles, respectively. Heated CCs (CCh) during sputtering showed improved cycle stability compared to the ones with no heating (Figure 2b). The CC with thicker coating exhibited higher CE after 100 cycles: CEs of 9-CCh and 15-CCh were 90.3 % and 85.0 %, respectively. However, CE of 6-CCh dropped to 41.2 % compared to the one of 6-CC, 82.9 %. Additional heating for 5 min or 10 min further improved the CE of 15-CCh to 96.2 % and 95.1 %, respectively, while the CE of 9-CCh deteriorated after additional heating was applied. It appears that the substrate heating during coating tends to improve the CE yet it deteriorates when coating was too thin. Overall, 15-CCh5 exhibited the most stable CE up to 130 cycles while CE of 15-CCh10 dropped after 100 cycles.

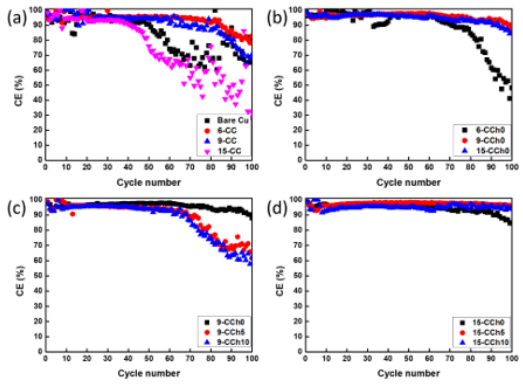

Figure 2. Comparison of Coulombic efficiency (CE) of Cu CC with 6 nm, 9 nm, 15 nm $PdTe_2$ deposited (a) with and (b) without heating at 200 °C, and additional 5 min and 10 min heated after deposition of (c) 9 nm $PdTe_2$ and (d) 15 nm $PdTe_2$.

Nucleation overpotential of $PdTe_2$ coated CC

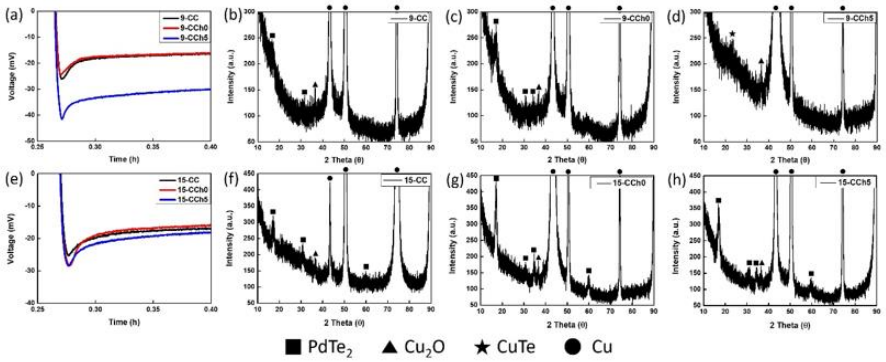

Figure 3. Nucleation overpotential on (a) 9 nm and (e) 15 nm coated CC without and with heating was measured at 0.1 mA/cm2. XRD profiles of 9 nm and 15 nm coated CC (b,f) without heating, (c,g) with heating during sputtering only, and (d,h) with heating during sputtering plus additional 5min heating after sputtering, respectively.

Nucleation overpotential on $PdTe_2$ coated Cu and crystal structure of the coating layer were investigated to understand the effect of heating process on electrochemical property. They clearly show the reason for improvement or deterioration of electrochemical property. While overpotential of 9-CC and 9-CCh0 are almost identical (25.8 and 23.5 mV respectively), it increased to almost double (41.6 mV) after additional heating as shown in Figure 3a. The increase of overpotential may be the reason for CE drop of 9-CC after heating. According to XRD analysis, $PdTe_2$ phase sustained in 9-CC and 9-CCh0 yet it almost disappeared and a new phase, CuTe, formed after additional 5 min heating as shown in Figure 3b-d. It means that some of Te in $PdTe_2$ reacted with Cu CC forming CuTe. It may be because the tendency for formation of chalcogenide vacancy in TMDC material and this tendency accelerated by heating. While the CuTe phase

form, reduction in thickness of $PdTe_2$ layer and its phase transformation to PdTe occurred. It may lead to reduction in the thickness and grain size, so that $PdTe_2$ or PdTe was not detected in XRD as shown in Figure 3d. Formation of CuTe phase is clearly confirmed from the XRD profile of 50 nm-thick $PdTe_2$ coating after heating for 30 min at the same temperature. No CuTe XRD peaks from the 15 nm-thick $PdTe_2$ deposited on SiOx substrate after heating for 90 min also confirms that formation of CuTe phase is resulted by the reaction between $PdTe_2$ and Cu CC. In case of 15 nm-coating, overpotential values are similar regardless of heating time. It was in the range of 25.4 mV to 28.4 mV. It should be because $PdTe_2$ phase was maintained after the heating as shown in Figure 3f-h.

Electrochemical properties of $PdTe_2$ coated current collectors

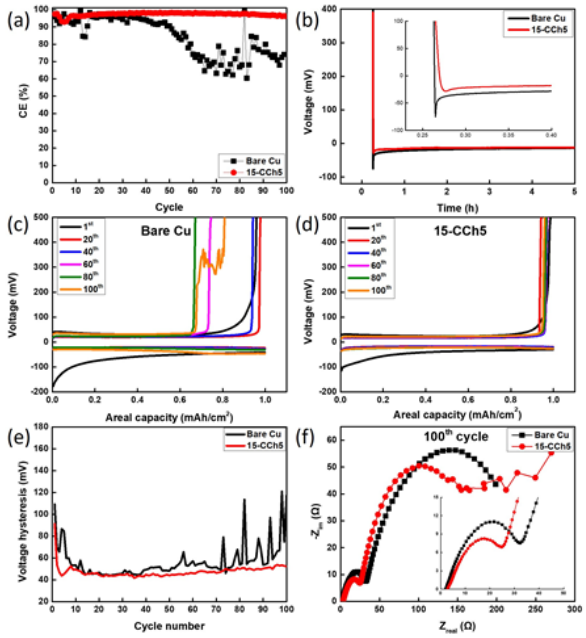

Figure 4. Comparison of cycling performance of bare Cu and 15-CCh5 in 1M LiTFSI, DME/DOL (1/1, v/v) and 2wt% $LiNO_3$ at 1 mA/cm^2. (a) CE graph for 100 cycles, (b) voltage-time curves during Li nucleation at 0.1 mA/cm2 for nucleation overpotential, voltage profiles of the 1st, 20th, 40th, 60th, 80th, and 100th cycle of (c) bare Cu and (d) 15-CCh5, (e) voltage hysteresis of bare Cu and 15-CCh5. Average voltages of charge and discharge were used for calculating the voltage hysteresis. (f) Nyquist plots after 100th discharging cycles

Significant improvement of electrochemical performance was attributed to enhancement of interfacial property. Direct comparison of CE of the bare Cu and 15-CCh5 in half-cell in Figure 4a shows that 15-CCh5 was stable up to 100 cycles while the bare Cu started to drop after about 50 cycles. Similar trend was observed from the charge–discharge curves at 1 mA/cm2 in Figure 4b and 4c. In the early stage of cycling (1st, 20th, and 40th cycle), the voltage profiles for the bare Cu (Figure 4b) and 15-CCh5 (Figure 4c) electrodes show similar lithium cycling. However, significant decrease in capacity is observed from the 60th cycle in

case of bare Cu while the capacity reduction in 15-CCh5 was negligible. The improved Li plating/stripping behaviors was due to improved interfacial property by the coating. The interfacial property was evaluated by measuring nucleation overpotential at the first cycle, voltage hysteresis during cycling, and EIS at 100th cycle. The nucleation overpotential of the bare Cu is dramatically reduced by the $PdTe_2$ coating layer from 75.1 mV to 28.4 mV (See Figure 4d). The reduced nucleation overpotential of 15-CCh5 may result in the improved CE and charge-discharge curves. The voltage hysteresis, voltage difference between the lithium plating and stripping, shows interfacial properties and charge transfer resistance.[48] Despite higher hysteresis in the beginning of the cycles because of the formation of the SEI layer, it decreases up to about 30 cycles for both the bare Cu and 15-CCh5 due to the creation of a greater surface area of lithium and lower total resistance. After the first 30 cycles, voltage hysteresis of bare Cu increased as cycle number increases because of unstable cycling and accumulation of resistive SEI. On the other hand, the voltage hysteresis for the $PdTe_2$ coated Cu electrode remained stable up to 100 cycles at an average value of 50 mV. Relatively lower interface impedance of 15-CCh5 than the one of bare Cu electrode after the 100th plating process verified by impedance spectroscopy (Figure 4f) also support the improvement of electrochemical performance in 15-CCh5.

Conclusion

Cu current collectors coated with $PdTe_2$ by sputtering exhibit considerably improve electrochemical performance. The $PdTe_2$ coating layer reduces nucleation overpotential by more than 50 % compared to the bare Cu and induces uniform current density distribution, that result in a dense and smoother morphology of Li deposits. Lower nucleation overpotential results in 20 % higher 1st discharge capacity and higher Coulombic efficiency in the early stage of the cycles. As cycle number increases, however, CE decreased. It may be due to dead lithium builds up on top of the current collectors regardless of existence of the $PdTe_2$ layer. The dead lithium results in comparable Coulombic efficiency in the full cells with bare Cu and $PdTe_2$ coated Cu after 20th cycles. Further study is necessary to minimize the reduction in CE as cycling.

(2) Exfoliation of 2D $NiTe_2$ Thin Films for Transparent Electrodes

Introduction

Transparent electrodes are an essential component in various electronic devices. Currently, indium-tin oxide (ITO) is widely used as a transparent electrode in devices because of its high transmittance (>80%) and low electrical resistivity (102 to 104 μΩ cm). As customers demand greater performance from the devices, transparent electrodes with superior optical and electrical properties are indeed required. Many attempts have been made to replace ITO with materials with lower electrical resistivity, such as graphene and silver. Graphene is one of the candidates for transparent electrodes because of its low theoretical sheet

resistance (10 – 30 Ω/sq) and superior optical transparency (~97.7%). Graphene has been intensively studied as an electronic material since it was discovered by Novoselov et al. in 2004. However, transparent electrodes fabricated by printed graphene or reduced graphene oxide showed higher sheet resistance than the theoretical electrode because of the reduction in carrier density during the fabrication process. Recently, transparent electrodes fabricated by printing Ag nanowires have more competitive advantages for commercialization due to their better electrical properties and ease of mass production. However, numerous problems of transparent electrodes fabricated by Ag nanowires, such as high junction resistance between wires, low adhesion of Ag nanowires on transparent substrates, and high haze attributed to their geometry, have yet to be solved.

Two-dimensional (2D) transition metal dichalcogenide (TMDC) materials have been considered potential candidates for transparent electrodes. TMDCs are materials with a generalized formula of MX2 (M: metals, X: chalcogens) and consist of TMDC layers. One TMDC layer is composed of one layer of transition metal sandwiched by two layers of chalcogen. The TMDC layers are all held by van der Waals force so that they can be exfoliated layer-by-layer, similar to graphene, by a liquid-phase exfoliation (LPE) process. TMDC thin films are mostly fabricated by two methods: printing the solution in which exfoliated TMDC layers are dispersed or depositing TMDC thin films by physical or chemical deposition methods followed by exfoliation to improve their transparency. Among the TMDC materials, NiTe2 was chosen as a material for transparent electrode in this study. $NiTe_2$ is a metallic TMDC, and its electrical resistivity is approximately 27 μΩ cm in a single crystal and 82 μΩ cm in a thin film. The electrical resistivity of $NiTe_2$ in a single crystal is comparable to the theoretical electrical resistivity of lead (22 μΩ cm), which is a main component of solder for electronic packaging. Also, the electrical resistivity of $NiTe_2$ is approximately one to three orders of magnitude lower than that of ITO. In addition to low electrical resistivity, the material cost for $NiTe_2$ is lower than other metallic 2D TMDCs, such as $PdTe_2$ or $PtTe_2$, which have comparable resistivity with $NiTe_2$. Thus, $NiTe_2$ is a promising material for transparent electrode. Previously, we studied the efficiency of exfoliating 2D $NiTe_2$ thin films deposited on glass substrates by sputtering in three co-solvents – mixing DI water with ethanol, acetone, or isopropyl alcohol. Among the three co-solvents, acetone–DI water vigorously separated $NiTe_2$ grains, which led to an increase in transmittance, but the sheet resistance rapidly increased. Ethanol–DI water led to layer-by-layer exfoliation, minimizing the increase in sheet resistance. Based on the previous result, it can be expected that transmittance further increases by carefully combining these two exfoliation mechanisms.

In this study, we optimized the mixing ratio of three solvents (ethanol:acetone:DI water = 2:4:4, 3:3:4, and 4:2:4 by volume) for the LPE process to achieve the maximum efficiency of exfoliation. The combination of the two mechanisms, separation and layer-by-layer exfoliation, led to an improvement in the transmittance of the NiTe2 thin film while keeping the electrical resistance low, i.e. high transmittance/resistance ratio. To better understand the two mechanisms, transmittance profiles of $NiTe_2$ after the LPE process for various time periods and polarization and dispersion ratios (p/d ratio) of the three mixed solvents were analyzed. We believe that the combination of the two exfoliation mechanisms by precisely controlling the mixing ratio of the solvents is a straightforward way to improve the efficiency of exfoliating 2D thin films on glass

substrates.

Results and Discussion

The transmittance and sheet resistance of $NiTe_2$ thin films varied after the 8-hour LPE process depending on the mixing ratio of ethanol, acetone and DI water. The formation of $NiTe_2$ phase in the sputtering target and the deposited thin films was confirmed by XRD. The XRD profile for the target was matched with the ICSD database (no. 01-089-2503) as shown in Fig. 1(a). The XRD profile of $NiTe_2$ thin film in Fig. 1(b) showed only (001) and (112) diffraction peaks due to the thickness yet it proved that the thin film had a preferred texture in which the basal plane was parallel with the substrate. The thickness of the $NiTe_2$ thin film deposited by RF sputtering was approximately 7 nm, and its transmittance was 59.6 ± 2.7%. Transmittance greatly improved to 68.4 ± 2.4% after the LPE process for 8 hours in the solvent in which the mixing ratio (by volume) of ethanol, acetone and DI water was 3:3:4 (3-3-4) as shown in Fig. 1(c). The transmittance after LPE in two other solvents whose mixing ratios were 2:4:4 (2-4-4) and 4:2:4 (4-2-4) were 66.5 ± 2.5% and 67.4 ± 2.0%, respectively. The values of transmittance and its error were the average value of transmittance from 380 nm to 700 nm wavelength and their standard deviation, respectively. In addition to the transmittance, sheet resistance also increased after the LPE process, as shown in Fig. 1(d). Reduction in the thickness of the NiTe2 thin film by exfoliation should be the main reason for the increase in sheet resistance. The sheet resistance of the $NiTe_2$ thin film before the LPE process was 190.2 ± 15.0 ohm/sq and increased to 440.2 ± 43.5 after LPE in 3-3-4, which was slightly higher than that after the LPE process in 2-4-4 (426.3 ± 15.6 ohm/sq) and 4-2-4 (421.1 ± 5.6 ohm/sq), although they were all in the error range. To further evaluate the effect of the LPE process on the electrical properties of the thin film, electrical resistivity, one of the intrinsic properties of the material, was compared. The electrical resistivity (ρ) was obtained by sheet resistance multiplied by the average thickness estimated by transmittance (Eq. 1 and 2).

$$\mathrm{I} = I_0 e^{-\alpha x} \qquad \text{Eq.1}$$

$$-\frac{\ln(\mathrm{I}/I_0)}{\alpha} \propto x \qquad \text{Eq.2}$$

where I, I0, α, and x are the light intensity at a depth of x, initial light intensity, absorption coefficient, and depth of light transmitted, respectively. The α value for $NiTe_2$ was 0.074 nm-1 that was calculated using the Eq.1 where I and x are thickness and transmittance of the as-deposited $NiTe_2$ thin film. The thickness of $NiTe_2$ thin films after LPE process was estimated by the natural log value of transmittance divided by α in Eq.2. The calculated ρ using the estimated thickness are summarized in Fig. 1(e). The thin film exfoliated in 3-3-4 and 4-2-4 showed comparable ρ, while the one exfoliated in 2-4-4 exhibited approximately 4% higher ρ than the others. Electrical resistivity is one of the material's intrinsic properties and should be constant regardless of thickness. The difference in ρ despite the same material means that variation in the solvent mixing ratio influenced not only the thickness but also the morphology of the thin films during the LPE process. Variation in the film morphology may induce an increase in resistance. Using the ρ values, the ratio

of transmittance/ρ (T/R) was compared in Fig. 1(f) to verify which mixed solvent is more effective for exfoliation of the $NiTe_2$ thin film on a glass substrate. The higher T/R is attributed to the higher transmittance and lower resistance that are essential for transparent electrodes. Based on the T/R ratio, 3-3-4 exhibited higher efficiency for the LPE process than the two others. A higher T/R ratio after the LPE in 3-3-4 means that transmittance improved while degradation of the $NiTe_2$ thin film was effectively restrained during the LPE process.

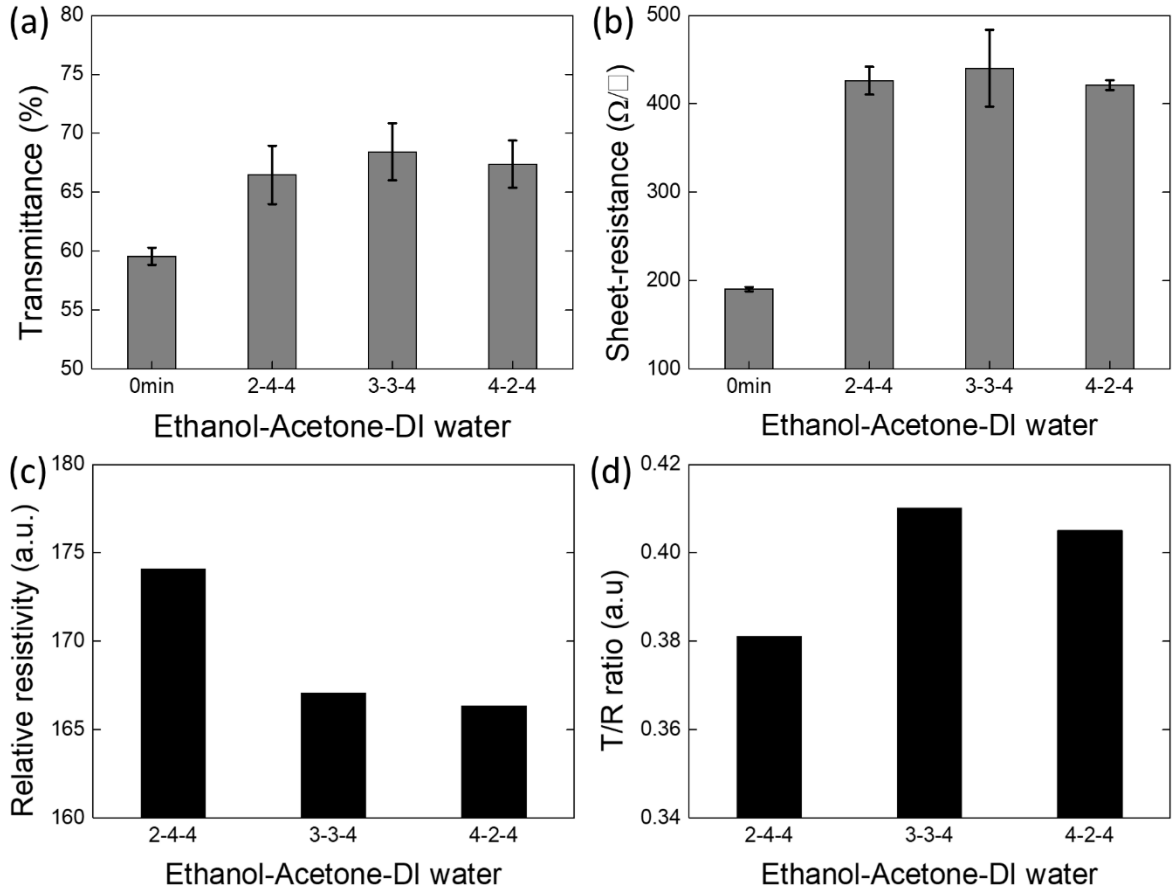

Fig. 1. XRD profiles of (a) the $NiTe_2$ sputtering target and (b) deposited $NiTe_2$ thin film. (c) Transmittance, (d) sheet resistance, (e) resistivity (ρ), and (f) transmittance/ρ ratio of $NiTe_2$ thin films after liquid-phase exfoliation (LPE) for 8 hours.

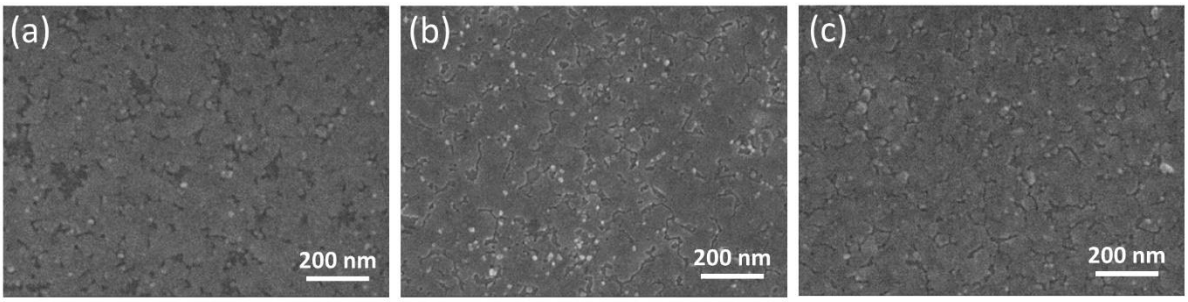

Fig. 2. SEM images of the top surface of $NiTe_2$ thin films after the LPE process for 8 hours in mixed solvents of (a) 2-4-4, (b) 3-3-4, and (c) 4-2-4. The separated areas after LPE process were indicated by the yellow arrows.

SEM images of the top surface of the $NiTe_2$ thin films after the LPE process in the three mixed solvents apparently showed that the difference in mixing ratio of the solvents led to divergence in the surface morphology of the thin films. After the LPE process for 8 hours in 2-4-4, the $NiTe_2$ thin film was partially separated from the glass substrate, and the size of the individual separated area was approximately 300 nm2, as shown in Fig. 2(a). This size decreased to ~100 nm2 in 3-3-4, and these areas were located mostly along the grain boundaries after the LPE process for 8 hours in 4-2-4. This is supported by our previous result [13]: the co-solvent of acetone and DI water (0-6-4, acetone:DI water = 6:4 by volume) exhibited more vigorous separation of $NiTe_2$ grains than the co-solvent with ethanol (6-0-4, ethanol:DI water = 6:4 by volume). The $NiTe_2$ exfoliated in 0-6-4 exhibited higher transmittance because a fraction of light passed through the separated areas without absorption. However, the sheet resistance also sharply increased because a partially separated thin film may increase the electron path, i.e. increase the tortuosity. In contrast, 6-0-4 led to similar transmittance compared to that in 0-6-4, although the separated area was smaller. In addition, it led to a sheet resistance lower than 0-6-4. This proved that layer-by-layer exfoliation operated more actively in 6-0-4. Based on the previous result, both separation and layer-by-layer exfoliation were expected to operate on NiTe2 in the three mixed solvents, among which 3-3-4 maximized the exfoliation efficiency while suppressing the increase in resistance according to its higher T/R ratio. Furthermore, 3-3-4 improved the exfoliation rate: it reduced the total LPE process time from 12 hours to 8 hours to achieve equivalent transmittance compared to the previous result (3-3-4: 68.4% after 8 hours vs. 6-0-4: 67.8% after 12 hours of LPE).

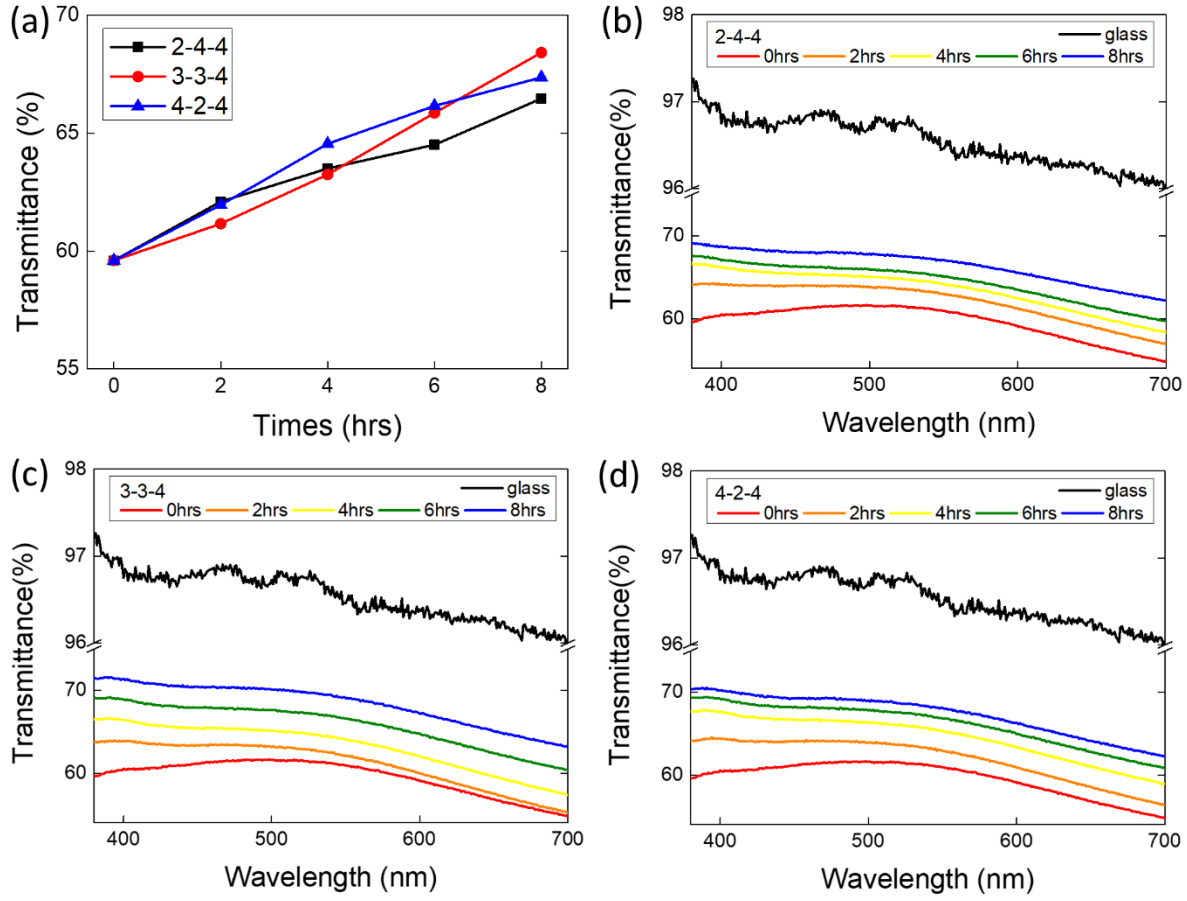

Fig. 3. (a) Average transmittance of $NiTe_2$ thin films as a function of LPE process time, and transmittance profiles of $NiTe_2$ thin films exfoliated in (b) 2-4-2, (c) 3-3-4, and (d) 4-2-4 measured in the visible light range (380 nm to 700 nm). Red, orange, yellow, green, blue, and black lines in (b, c, d) indicate transmittance before LPE, after LPE for 2, 4, 6, 8 hours, and transmittance spectra of glass substrate.

The average transmittance as a function of LPE time in Fig. 3(a) shows that transmittance almost linearly increased as LPE time increased in the three mixed solvents. In the early stage of the LPE process (less than 4 hours), transmittance increased faster (steeper slope) in 2-4-4 or 4-2-4 than 3-3-4, yet it increased faster in 3-3-4 than others in the later stage of the LPE process (longer than 6 hours). The transmittance profiles after various LPE time periods in Fig. 3(b-d) also showed that transmittance increased as LPE time increased. Regardless of the mixing ratios and LPE time periods, the transmittance at shorter wavelength (~380 nm) is higher than that at longer wavelength (~700 nm). This should be because the intensity profile of the light source for the measurement (black line in Fig. 3(b-d)), which transmitted the glass substrate only, also exhibited higher intensity at shorter wavelength. The measured transmittance was proportional to the intensity profile of the light source used for the measurement.

To investigate the effect of the solvent mixing ratio on exfoliation mechanisms operated on the $NiTe_2$ thin films, difference in transmittance between the measurements made before and after additional 2-hour exfoliation was compared: the profiles of transmittance after exfoliation for 2, 4, 6, and 8 hours were

subtracted by the one after exfoliation for 0, 2, 4, and 6 hours, respectively, and they are provided in Fig. 4. It clearly shows a marked improvement in transmittance at shorter wavelength in the early stage of the LPE process (up to 4 hours) in the three solvents. The higher increase in transmittance at shorter wavelength (the black lines in Fig. 4(a), (b) and (c)) should be due to a fraction of the light source transmitted to the thin films without absorption. The light source had a higher intensity at shorter wavelength. The only possible explanation for this is that the $NiTe_2$ thin film was partially separated from the substrate in the early stage of the LPE process. A certain percentage of the light source, which is proportional to the fraction of the separated area, went through the separated areas without being absorbed by $NiTe_2$. If the thickness of the thin film reduced uniformly over the entire area of the thin film, the difference in transmittance between before and after an additional 2 hours of exfoliation should be the same in the wavelength range regardless of the intensity variation of the light source. Partially separated $NiTe_2$ thin films were confirmed by SEM, as shown in Fig. 2. When the exfoliation time was longer than 6 hours, the transmittance almost uniformly increased over the wavelength range of 380 nm to 700 nm. This confirmed that layer-by-layer exfoliation was the dominant mechanism in the later stage of the LPE process. Based on the progress of transmittance, it was revealed that partial separation of the $NiTe_2$ thin film from the substrate followed by layer-by-layer exfoliation took place in the three mixed solvents.

Layer-by-layer exfoliation was the main exfoliation mechanism for the later stage of LPE, as discussed above. The increasing rate of the transmittance of $NiTe_2$ in the later stage of LPE (4 – 8 hours) was carefully examined by comparing the transmittance at 380 nm wavelength. The increasing rate of transmittance during the LPE for 4 – 6 hours in 3-3-4 was faster than the two other solutions: an increase of 2.5% in 3-3-4 and 1.0% and 1.6% in 2-4-4 and 4-2-4, respectively. The increase in transmittance during the LPE for 6 – 8 hours exhibited the same trend: the increase in transmittance in 3-3-4 (2.5%) was higher than that in 2-4-4 (1.5%) and in 4-2-4 (1.1%). Increasing the rate of transmittance confirmed that the 3-3-4 solvent had a higher efficiency for layer-by-layer exfoliation of the $NiTe_2$ thin film.

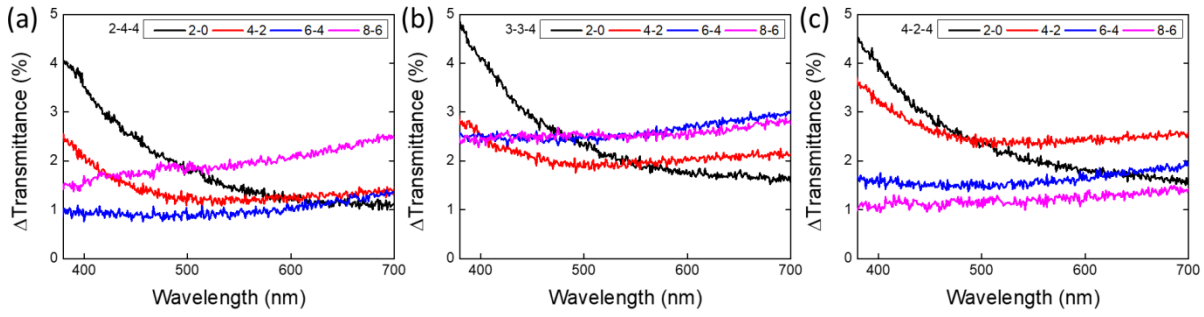

Fig. 4. Difference in transmittance of $NiTe_2$ thin films between the measurements made before and after an additional 2-hour LPE process in (a) 2-4-2, (b) 3-3-4, and (c) 4-2-4. The difference in transmittance was calculated by subtracting the transmittance profiles after LPE for 0, 2, 4, and 6 hours from the transmittance profiles for 2, 4, 6, and 8 hours, respectively.

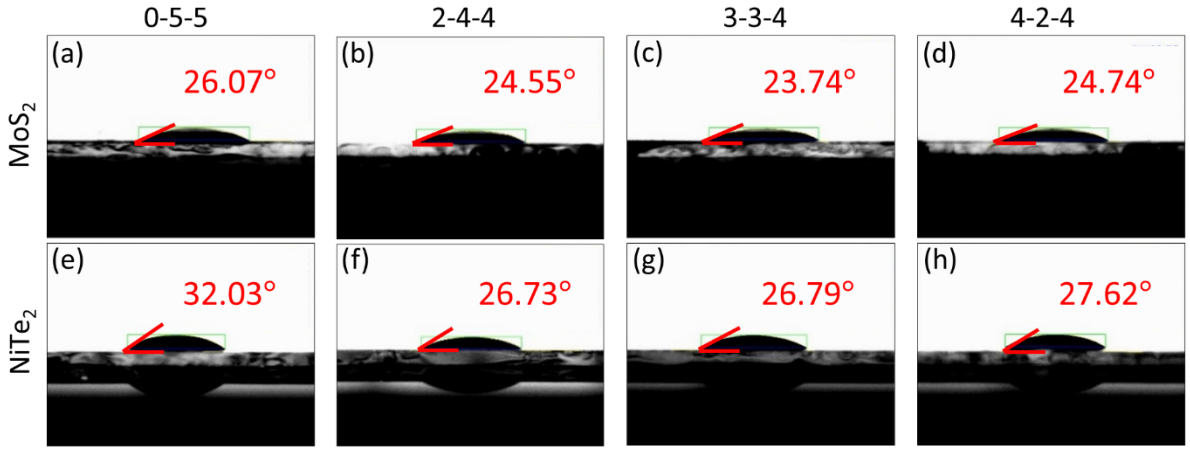

Fig. 5. Contact angles of (a, e) 0-5-5, (b, f) 2-4-4, (c, g) 3-3-4, and (d, h) 4-2-4 on (a, b, c, d) $NiTe_2$ and (e, f, g, h) MoS_2.

The improvement in transmittance as a function of LPE time discussed above clearly shows that the partially separating mechanism was mainly operated in the early stage, while the layer-by-layer mechanism was mainly operated in the later stage of LPE. The two mechanisms were more productively combined in 3-3-4. To investigate how the solvent mixing ratios influenced the two exfoliation mechanisms, the polarization and dispersion ratio (p/d ratio) of the $NiTe_2$ thin film and the three mixed solvents were evaluated by measuring the contact angles of the mixed solvents on $NiTe_2$. The contact angles of the mixed solvents on the MoS_2 thin film were also measured because contact angles on two different thin films were necessary to obtain the p/d ratio. It is well known that the efficiency of the LPE process maximizes when the surface tension between the solid and liquid (σ_{sl}) is as low as possible. A lower σ_{sl} value can be achieved when the p/d ratios of solid and liquid are closer together according to Eq. 3.

$$\sigma_{sl} = \sigma_s + \sigma_l - 2\left(\sqrt{\sigma_s^d \cdot \sigma_l^d} + \sqrt{\sigma_s^p \cdot \sigma_l^p}\right)$$

$$= \sigma_s^d + \sigma_s^p + \sigma_l^d + \sigma_l^p - 2\left(\sqrt{\sigma_s^d \cdot \sigma_l^d} + \sqrt{\sigma_s^p \cdot \sigma_l^p}\right) \quad \text{Eq. 3}$$

$$\sigma_{sl} = \sigma_s - \sigma_l cos\theta = \sigma_s^d + \sigma_s^p - \left(\sigma_l^d + \sigma_l^p\right)cos\theta \quad \text{Eq. 4}$$

$$\frac{\sigma_l(1+cos\theta)}{2\sqrt{\sigma_l^d}} = \sigma_s^d + \sqrt{\frac{\sigma_l^p}{\sigma_l^d}} \cdot \sqrt{\sigma_s^p} \quad \text{Eq. 5}$$

where θ, σ_s, σ_l, and σ_{sl} are the contact angle, surface tension of solid, liquid, and between solid and liquid phase, respectively, and p and d indicate the polar component and dispersive component, respectively. If Eq. 3 is combined with Young's equation (Eq. 4), Eq. 5 can be achieved. To achieve the values of σ_l^d and σ_l^p for

the three mixed solvents, another solid material with known σ_s^d and σ_s^p and one more solvent with known σ_l^d and σ_l^p are necessary for the calculation. MoS_2 and the co-solvent (1:1 volume ratio of acetone and DI water, 0-5-5) were chosen in this study. The p/d ratio of MoS_2 (0.45) and σ_l^d (22.26) and σ_l^p (10.90) of 0-5-5 were reported previously. First, individual values of σ_s^d and σ_s^p of MoS_2 were calculated by inserting the σ_l^d and σ_l^p of 0-5-5 and the measured contact angle of 0-5-5 on MoS_2 into Eq. 5. The measured contact angles are provided in Fig. 5. The results of the calculation are summarized in Table 1. Second, σ_s^d and σ_s^p of $NiTe_2$ were obtained by using the σ_l^d and σ_l^p of 0-5-5 and the p/d ratio of $NiTe_2$ (2.06) reported in our previous study. The obtained σ_s^d and σ_s^p of $NiTe_2$ are 4.17 and 8.58, respectively. Third, σ_l^d and σ_l^p for each of the three mixed solvents were achieved by measuring their contact angles on $NiTe_2$ and MoS_2. When the measured contact angle of the individual mixed solvent on $NiTe_2$ (or MoS_2) and σ_s^d and σ_s^p of $NiTe_2$ (or MoS_2) were inserted into Eq. 5, this yielded a set of two equations with two unknown variables (σ_l^d and σ_l^p). Finally, σ_l^d and σ_l^p for the individual mixed solvents were achieved by solving the set of two equations. The σ_l^d and σ_l^p of the three mixed solvents were calculated using the average values of the contact angles, and the results are summarized in Table 1. The p/d ratio of 4-2-4 (0.971) was closer to that of $NiTe_2$ (2.06) than those of 2-4-4 (0.941) and 3-3-4 (0.950).

Table 1. Measured contact angles (θ) of co-solvent (0-5-5, acetone:DI water = 1:1 by volume) and three solutions on $NiTe_2$ and MoS_2, and polarization (σ^p) and dispersion (σ^d) component and p/d ratio (σ^p/σ^d) of the 0-5-5, 2-4-4, 3-3-4, 4-2-4, $NiTe_2$, and MoS_2.

	$NiTe_2$							MoS_2			
	θ	σ_l^p	σ_l^d	σ_l^p/σ_l^d	σ_s^p	σ_s^d	σ_s^p/σ_s^d	θ	σ_s^p	σ_s^d	σ_s^p/σ_s^d
0-5-5	32.4 ± 2.9	10.90	22.26	0.49	8.58	4.17	2.06	26.2 ± 1.4	2.50	5.56	0.45
2-4-4	26.5 ± 2.6	13.66	14.52	0.941				23.3 ± 3.7			
3-3-4	26.7 ± 2.0	13.67	14.55	0.950				23.9 ± 0.6			
4-2-4	27.2 ± 1.2	13.94	14.36	0.971				25.0 ± 1.2			

It could be expected that 4-2-4 would lead to faster exfoliation and thus higher transmittance because the p/d ratio of 4-2-4 is closer to the p/d ratio of NiTe2. However, empirical results showed that 3-3-4 led to higher transmittance than 4-2-4. The discrepancy between the expected transmittance based on the p/d ratios and the measured transmittance was attributed to the form of $NiTe_2$. The effect of the p/d ratio on the exfoliation of 2D materials was examined by using particles in a previous study. Particles generally have a large surface-to-volume ratio, so the area where interslabs (inter-layer space) of 2D materials are exposed to the liquid solvent is relatively large. Thus, the solvent is easily intercalated into the interslabs for exfoliation. Because the $NiTe_2$ was in the form of a thin film, however, the area where interslabs are exposed to solvent is strictly limited compared to particles. If the basal plane of grains in the thin film is parallel to the substrate, the interslabs are blocked by neighboring grains, which reduces the efficiency of exfoliation.

When some grains are separated from the glass substrate, the probability that the interslab area is exposed to the solvent increases. Although more separation led to more suitable conditions for layer-by-layer exfoliation in the case of 2-4-4, the relatively lower capability for layer-by-layer exfoliation due to the larger difference in the p/d ratio between $NiTe_2$ and 2-4-4 led to lower transmittance than the two other solvents after the 8-hour LPE. In contrast, a lower content of acetone in 4-2-4 resulted in separation along the grain boundaries only, yet it increased transmittance due to the higher capability of layer-by-layer exfoliation. 4-2-4 exhibited a smaller difference in the p/d ratio with $NiTe_2$. Therefore, 3-3-4 properly separated $NiTe_2$ grains from the substrate, which increased transmittance while effectively suppressing the increase in electrical resistance in the early stage of the LPE process. This was confirmed by the lower ρ value and higher T/R ratio after the LPE process (Fig. 1). The partially separated morphology (Fig. 2(b)) and its p/d ratio of 0.950 increased the exfoliation rate in the later stage of the LPE process, as shown in Fig. 3(a). To further improve the transmittance of 2D thin films and remarkably reduce the LPE time period, a technique to deposit thinner yet still continuous $NiTe_2$ films on glass substrates should be developed by employing interface engineering. NiTe2 tends to grow on glass in Volmer-Weber mode (island growth) due to the interface energy between NiTe2 and glass. If the thickness of the as-deposited $NiTe_2$ thin film is much thinner than 7 nm, we believe that not only ITO-level transmittance and sheet resistance but also a reduction in the LPE period will be achieved.

Conclusion

The efficiency of exfoliating 2D $NiTe_2$ thin films deposited on glass substrates was optimized by varying the mixing ratio of three solvents in solution for the LPE process. Three mixed solvents with different mixing ratios of acetone, ethanol, and DI water (acetone:ethanol:DI water = 2:4:4, 3:3:4, and 4:2:4 by volume) were used for the LPE process. Among the three mixed solvents, 3-3-4 exhibited the highest exfoliating efficiency. It increased the transmittance of the $NiTe_2$ thin film from 59.6% to 68.4% after the 8-hour LPE process while more effectively suppressing the increase in electrical resistance. It also reduced the LPE processing time to achieve equivalent transmittance. The transmittance was improved by two exfoliation mechanisms: partial separation of the $NiTe_2$ thin film from the substrate and layer-by-layer exfoliation of the 2D $NiTe_2$ thin film. The 3-3-4 solvent led to moderate separation of the $NiTe_2$ thin film from the substrate in the early stage of LPE, which increased transmittance but did not sharply increase the electrical resistance. Once some of the $NiTe_2$ grains were separated, the area where the interslabs of the 2D materials were exposed to the solvent was enlarged. It provided a more supportive environment for layer-by-layer exfoliation. In the later stage of LPE, a smaller difference in the p/d ratio between $NiTe_2$ and 3-3-4 led to a further increase in the transmittance of $NiTe_2$ by layer-by-layer exfoliation.